CrystEngComm

Accepted Manuscript

ROYAL SOCIETY OF CHEMISTRY

rsc.li/crystengcomm

CrystEngComm

Paper

4-Cyanopyridine, a versatile mono- and bidentate ligand. Crystal structures of related coordination polymers determined by X-ray powder diffraction.

Received 00th xx 2017
Accepted 00th xx 2017

DOI: 10.1039/x0xx00000x

www.rsc.org/

Haishuang Zhao,[a, b] Alexander Bodach,[a] Miriam Heine,[a] Yasar Krysiak,[a, b] Jürgen Glinnemann[a], Edith Alig[a], Lothar Fink,*[a] and Martin U. Schmidt[a]

4-Cyanopyridine (4-CNpy, also known as isonicotinonitrile) can act as a monodentate ligand in transition metal complexes *via* the pyridine nitrogen atom (N_{py}), or as a bidentate ligand *via* both nitrogen atoms (N_{py} and N_{CN}), resulting in a linear bridge between two metal atoms. Seven new polymeric transition metal compounds, $[CuCl_2(4\text{-CNpy})]_n$ (**1b**), $[MnCl_2(4\text{-CNpy})]_n$ (**2b**), $[NiCl_2(4\text{-CNpy})_2]_n$ (**3a**), $[NiCl_2(4\text{-CNpy})]_n$ (**3b**), $[CoBr_2(4\text{-CNpy})_2]_n$ (**4a**), $[NiBr_2(4\text{-CNpy})_2]_n$ (**5a**) and $[NiBr_2(4\text{-CNpy})]_n$ (**5b**) are reported. Compounds **1b**, **2b**, **3b** and **5b** were obtained from the corresponding $[M(II)X_2(4\text{-CNpy})_2]_n$ compounds by careful thermal decomposition under controlled conditions. Compounds **3a**, **4a** and **5a** were synthesized from 4-cyanopyridine and transition metal halides. For all compounds, IR-spectroscopy was used to distinguish between mono- or bi-coordination of the 4-cyanopyridine ligand: in bi-coordinated compounds the asymmetric stretching vibrations of the cyano group ν_{as}(C≡N) are shifted to higher frequencies. All crystal structures were determined from X-ray powder diffraction data. Compounds **1b**, **3a**, **4a** and **5a** consist of polymeric chains of octahedra (double chains for **1b**; single chains for **3a**, **4a** and **5a**), in which 4-cyanopyridine acts as a monodentate ligand *via* the N_{py} atom. Compound **1b** exists in two polymorphs, a triclinic (**α-1b**) and a monoclinic phase (**β-1b**); both exhibit a strong Jahn-Teller distortion of the $CuCl_5N$-octahedra. On the other hand, **2b**, **3b** and **5b** exhibit layered structures, in which the 4-cyanopyridine acts as a bidentate ligand. Both nitrogen atoms coordinate to metal atoms, resulting a linear *M*(II)-py-C≡N-*M*(II) bridge. These are the first examples of Mn and Ni compounds, in which two 3d metal atoms are connected by a 4-cyanopyridine bridge. Due to the linearity of this bridge, 4-cyanopyridine lends itself to the construction of new metal organic frameworks.

Introduction

Coordination polymers with 4-cyanopyridine as ligand belong to a class of materials which have attracted much attention due to their potential properties with applications in many fields[1–10], e.g., adsorption, catalysis, optical and magnetic materials, and separation.

The neutral ligand 4-cyanopyridine (4-CNpy, also known as isonicotinonitril) contains two atoms with donor functions: the N_{py} atom and the N_{CN} atom and has therefore the potential to form linear *M*(II)-py-C≡N-*M*(II) bridiges, which may be used to construct coordination polymers or even metal organic frameworks. In spite of these promising abilities 4-cyanopyridine has relatively rarely been used for the design of transition metal polymers and networks. The Cambrige Structure Database (CSD)[11,12] contains only about 140 crystal structures of transition metal complexes with 4-cyanopyridine. Structures with bridging 4-cyanopyridine groups are very rare. In the CSD there are only eleven structures with bridging 4-cyanopyridines between two metal atoms, each one with Cu[13–16], Ru[17], Rh[18], Ag[19,20] and Cd[21,22]. Astonishingly, bridging 4-cyanopyridine ligands have not been observed in Mn and Ni complexes, hitherto. When 4-cyanopyridine acts as a monodentate ligand, the N_{py} atom coordinates due to its stronger Lewis-base character. This leads to the question, whether the monodentate or the bidentate behaviour can be controlled *via* the 'concentration' of the ligand during the preparation of a compound. Whether one-dimensional coordination polymers or higher dimensional networks will occur, should depend on the chemical composition as well as on the donating ability of the donors.

In previous work, using pyridine instead of 4-cyanopyridine, we investigated the compounds $[M(II)Cl_2(pyridine)_x]_n$ (*M*(II) = Cu, Ni) with three different metal-ligand ratios: x = 2, 1, 2/3.[23] In all these compounds, pyridine acts as a terminal ligand. The metal atoms are connected by the Cl atoms into single chains for x = 2, double chains for x = 1 and triple chains for x = 2/3. In the present work, we investigated the ability of 4-cyanopyridine to act as a mono- or bidentate ligand, *i.e.* to coordinate the metal atom as a terminal or as a bridging ligand, depending on the metal-ligand ratio, on the type of metal and halide atom. Therefore, we synthesized compound $[M(II)X_2(4\text{-CNpy})_x]_n$ with *M*(II) = Cu, Mn, Ni, Co; *X* = Cl, Br and x

[a] Institute of Inorganic and Analytical Chemistry, Goethe University, Max-von-Laue-Str. 7, 60438 Frankfurt am Main, Germany. E-Mail: fink@chemie.uni-frankfurt.de; Fax: +49 69798 29235; Tel: +49 69798 29123
[b] Present address: Institute of Inorganic Chemistry and Analytical Chemistry, Johannes Gutenberg University, Jakob-Welder-Weg 11, 55128 Mainz, Germany.

†Electronic Supplementary Information (ESI) available: DTA/TG curves of **3a**, **4a** and **5a**; results of DTA/TG measurements of **1a** - **5a**; combined Rietveld plot of **1b** (sample **2**); fragment of crystal structure **3b**, schematic representation for preparation of compound **1b**; IR spectra of all 4-cyanopyridine compounds. Results of quantitative Rietveld analysis for **1b**. See DOI: 10.1039/x0xx00000x

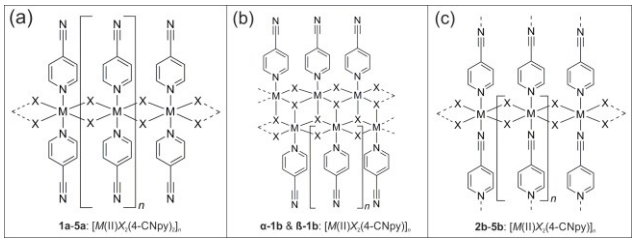

Scheme 1 Connectivity pattern of investigated coordination polymers.

= 1, 2 (Scheme 1). Compounds with a metal-ligand ratio of 1:2 were synthesized from 4-cyanopyridine and the corresponding metal dihalides. The compounds with a metal-ligand ratio of 1:1 were obtained from the corresponding 1:2 compounds by thermal decomposition under controlled conditions. In order to determine, if the 4-cyanopyridine motif is coordinated as a mono or bidentate ligand, IR-spectra of all compounds were recorded and the frequencies of the asymmetric stretching vibrations of the cyano groups ν_{as}(C≡N) were analyzed.

Only the crystal structures of **1a** and **2a** have previously been determined.[24] In both structures, 4-cyanopyridine molecule acts as a monodentate ligand. All other compounds are new. We were unable to obtain single crystals of the new compounds. Especially the 1:1 compounds (**1b**, **2b**, **3b**, **5b**) prepared by thermal decomposition were always microcrystalline or nanocrystalline powders. Hence, all crystal structures were determined by X-ray powder diffraction.

Results and discussion

Synthesis and thermal investigation

The compounds with a metal-ligand ratio of 1:2, $[M(II)X_2(4\text{-CNpy})_2]_n$ (**1a** - **5a**), were synthesized using 4-cyanopyridine and the corresponding anhydrous metal dihalides in alcoholic solution. The thermal behaviour of these compounds was investigated by differential thermal and thermogravimetric analyses (DTA/TG) under nitrogen atmosphere. Compounds $[M(II)X_2(4\text{-CNpy})]_n$ (**1b - 5b**), were prepared by thermal decomposition of the corresponding $[M(II)X_2(4\text{-CNpy})_2]_n$ at an appropriate temperature. $[CuCl_2(4\text{-CNpy})_2]_n$ (**1a**) slowly releases one equivalent of 4-cynopyridine between 200 °C and 270 °C and forms compound $[CuCl_2(4\text{-CNpy})]_n$ (**1b)**, which decomposes to 4-cyanopyridine and $CuCl_2$ at 314 °C (Fig. 1a; Table S1). Similarly, $[NiCl_2(4\text{-CNpy})_2]_n$ (**3a**) transforms to $[NiCl_2(4\text{-CNpy})]_n$ (**3b**) between 200 °C and 260 °C, which decomposes to $NiCl_2$ and 4-cynopyridine finally at 374 °C (Fig. S1, Table S1).

The TG curve of $[MnCl_2(4\text{-CNpy})_2]_n$ (**2a**) shows three steps of weight loss (Fig. 1b, Table S1), which correspond to the endothermic signals in the DTA curve. The first endothermic signal is assigned to the liberation of the first 4-cyanopyridine molecule at 253 °C to form $[MnCl_2(4\text{-CNpy})]_n$ (**2b**), according to Eq. (1). The second endothermic signal at 318 °C is attributed to the decomposition of this intermediate compound to form $[MnCl_2(4\text{-CNpy})_{1/3}]_n$ (**2c**), according to Eq. (2). The remaining 4-cyanopyridine is released in the third decomposition step at 393 °C to leave $MnCl_2$, according to Eq. (3).

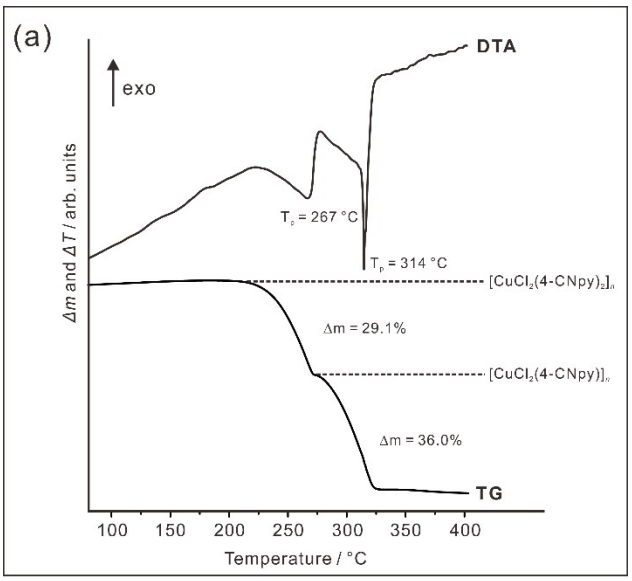

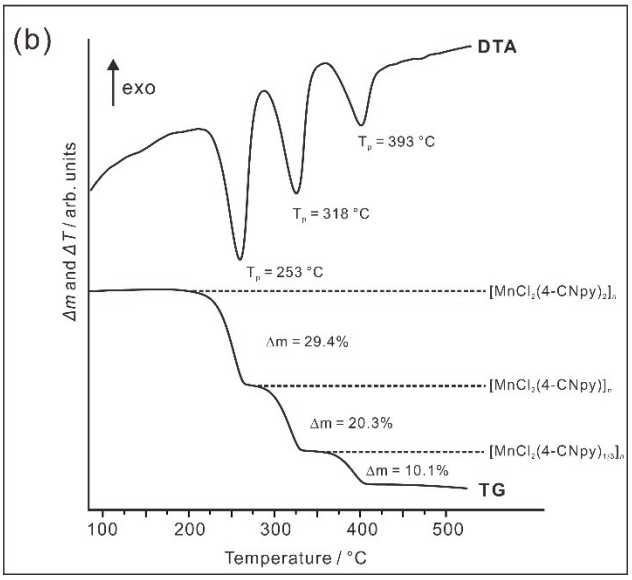

Fig. 1 DTA/TG curves of (a) $[CuCl_2(4\text{-CNpy})_2]_n$ (**1a**) and (b) $[MnCl_2(4\text{-CNpy})_2]_n$ (**2a**).

$$MnCl_2(4\text{-CNpy})_2 \rightarrow MnCl_2(4\text{-CNpy}) + 4\text{-CNpy} \quad (1)$$

$$MnCl_2(4\text{-CNpy}) \rightarrow MnCl_2(4\text{-CNpy})_{1/3} + 2/3(4\text{-CNpy}) \quad (2)$$

$$MnCl_2(4\text{-CNpy})_{1/3} \rightarrow MnCl_2 + 1/3(4\text{-CNpy}) \quad (3)$$

Similarly, $[CoBr_2(4\text{-CNpy})_2]_n$ (**4a**) reacts to $[CoBr_2(4\text{-CNpy})]_n$ (**4b**) at 241 °C, which releases two thirds of the remaining ligand to form $[CoBr_2(4\text{-CNpy})_{1/3}]_n$ (**4c**) at 339 °C. Finally, at 374°C, $CoBr_2$ remains (Fig. S2, Table S1). $[NiBr_2(4\text{-CNpy})_2]_n$ (**5a**) reacts to $[NiBr_2(4\text{-CNpy})]_n$ (**5b**) at 237 °C, which decomposes to $NiBr_2$ and 4-cyanopyridine at 374°C (Fig. S3, Table S1). Various attempts to synthesize pure phases of $[MnCl_2(4\text{-CNpy})_{1/3}]_n$ (**2c**) and $[CoBr_2(4\text{-CNpy})_{1/3}]_n$ (**4c**) failed.

Investigation of the coordination of the cyano group by FT-IR

FT-IR-spectroscopy was used to investigate whether the cyano group coordinates to a metal atom or not. A shifted value of the asymmetric stretching vibration ν_{as}(C≡N) indicates that the cyano group coordinates to a metal atom, while a value similar

Table 1 Characteristic asymmetric stretching vibrations ν_{as}(C≡N) for 4-cyanopyridine and its coordination polymers.

Compound	ν_{as}(C≡N) /cm^{-1}
Cyanopyridine	2236-2243
Compounds with a metal:ligand ratio of 1:2	
$[CuCl_2(4\text{-}CNpy)_2]_n$ (**1a**)	2242
$[MnCl_2(4\text{-}CNpy)_2]_n$ (**2a**)	2241
$[NiCl_2(4\text{-}CNpy)_2]_n$ (**3a**)	2242
$[CoBr_2(4\text{-}CNpy)_2]_n$ (**4a**)	2234
$[NiBr_2(4\text{-}CNpy)_2]_n$ (**5a**)	2235
Compounds with a metal:ligand ratio of 1:1	
$[CuCl_2(4\text{-}CNpy)]_n$ (**1b**)	2243
$[MnCl_2(4\text{-}CNpy)]_n$ (**2b**)	2275
$[NiCl_2(4\text{-}CNpy)]_n$ (**3b**)	2288
$[CoBr_2(4\text{-}CNpy)]_n$ (**4b**)	2281
$[NiBr_2(4\text{-}CNpy)]_n$ (**5b**)	2298

to that of 4-cyanopyridine itself indicates that the cyano group remained unchanged, *i.e.* the 4-cyanopyridine coordinates only *via* the N atom of the pyridine ring.[25–27] In **1a** - **5a** and **1b**, the frequency is similar to the frequency of the noncoordinated 4-cyanopyridine (Table 1). In contrast, the asymmetric stretching vibration ν_{as}(C≡N) in **2b** - **5b** is shifted to higher values (Table 1). This reveals that 4-cyanopyridine forms a bridge between the metal atoms in these compounds while in all the other compounds a monodentate behaviour of the ligand is observed.

Structure determination from powder data

The crystal structures of **3a** - **5a**, **1b** - **3b** and **5b** were determined from X-ray powder data. (For details see Experimental Section). For ease of comparison of the individual crystal structures, the unit cell for all structures was set up in such a way that the metal-halogen polymeric chains are parallel to the ***c*** axis. For some of the crystal structures, this leads to non-standard space-group settings (*P*11*m* instead of *P*1*m*1 for **2b** and *P*112/*m* instead of *P*12/*m*1 for **3b** and **5b**). Selected crystallographic data are summarized in Table 2 and Table 3. Rietveld plots are shown in Fig. 4 (combined Rietveld refinement of **1b** sample **2** see Fig. S4 in the ESI). For $[CoBr_2(4\text{-}CNpy)]_n$ (**4b**) no reliable indexing of the powder diffraction data succeeded.

Polymorphism of 1b

For $[CuCl_2(4\text{-}CNpy)]_n$ (**1b**), the X-ray powder data were inconsistent. The compound was prepared three times, under slightly different conditions at 207 °C and 220 °C (see Experimental Section for details); the X-ray powder diagrams (measured at room temperature) show identical peak positions, but significantly different reflection intensities (Fig. 2). It turned out that compound **1b** exists in two polymorphic forms, **α-1b** and **β-1b**. All three samples contained a phase mixture with different amounts of the two polymorphs.

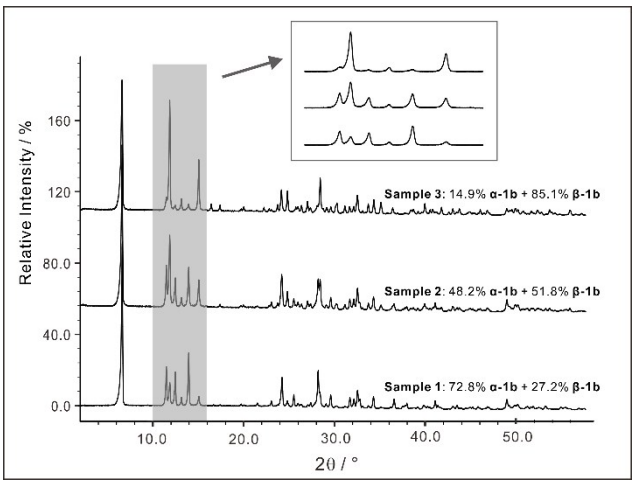

Fig. 2 X-ray powder patterns of three samples of compound **1b** (Cu $K\alpha_1$ radiation).

Powder data of the individual polymorphs were obtained by subtracting the data of the phase mixtures from each other. Subsequently the structure could be solved in a routine manner. Finally, the combined Rietveld refinements of both phases were performed, using the original powder diffraction data of polymorph mixtures. The monoclinic phase prefers to appear at a higher synthesis temperature. (For details see experimental section, Fig. 2 and Table S2.)

Monitoring the formation of α- and β-1b by temperature-dependent X-ray diffraction

The reaction from **1a** to **1b** was investigated by temperature-dependent X-ray diffraction, recording powder patterns from 170 °C to 250 °C in steps of 5 °C every 15 minutes. The 3D plot of the X-ray powder patterns (Fig. 3) confirms first structural changes at about 190 °C, corresponding to a decomposition of **1a** and the formation of **α-1b**. At about 220 °C this transformation is completed. In the DTA/TG measurement, where the heating rate is much faster (5 K/min), this reaction from **1a** to **1b** occurs between about 210 °C and 270 °C. Under further heating, additional changes are observed, starting at about 230 °C. These changes do not correspond to a further decomposition, but to the polymorphic phase transition from **α-1b** to **β-1b**. In the DTA curve this transformation is indicated as a shoulder at about 290°C (Fig. 1a).

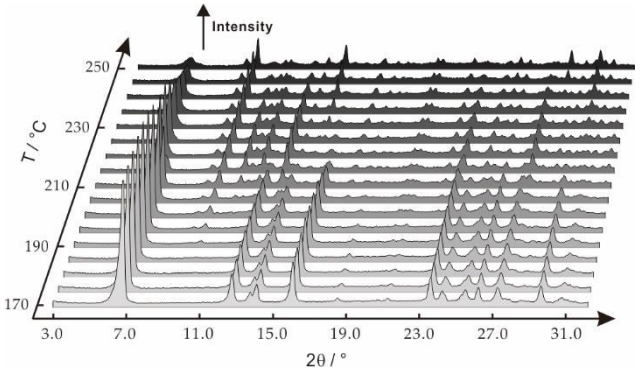

Fig. 3 Temperature dependent X-Ray powder diffraction diagrams of the thermal decomposition of compound **1a** (Cu $K\alpha_1$ radiation), yielding the triclinic phase (**α-1b**) firstly, which starts to transform to the monoclinic phase (**β-1b**) upon further heating.

Table 2 Selected crystallographic data and Rietveld refinement parameters for compounds **1a-5a**. In all structures the $[M(II)_2X_4]_n$ chains run along the ***c*** axis.

	1a [a]	**2a** [b]	**3a**	**4a**	**5a**
Compound	$[CuCl_2(4\text{-}CNpy)_2]_n$	$[MnCl_2(4\text{-}CNpy)_2]_n$	$[NiCl_2(4\text{-}CNpy)_2]_n$	$[CoBr_2(4\text{-}CNpy)_2]_n$	$[NiBr_2(4\text{-}CNpy)_2]_n$
CCDC number/CSD code	NESYOZ	NESYUF	1535275	1535270	1535271
Ref.	[24]	[24]	This work	This work	This work
Structure determined from	Single-crystal	Single-crystal	Powder	Powder	Powder
Formula	$C_{12}H_8Cl_2CuN_4$	$C_{12}H_8Cl_2MnN_4$	$C_{12}H_8Cl_2NiN_4$	$C_{12}H_8Br_2CoN_4$	$C_{12}H_8Br_2NiN_4$
MW /g·mol^{-1}	342.67	334.06	337.82	426.95	426.49
Crystal system	Monoclinic	Monoclinic	Monoclinic	Orthorhombic	Orthorhombic
Space group (No.)	*P* $2_1/n$ 1 1 (14)	*P* 1 $2_1/n$ 1 (14)	*P* 1 $2_1/n$ 1 (14)	*P n n m* (58)	*P n n m* (58)
a /Å	25.711(12)	26.640(5)	26.4504(7)	26.8461(15)	26.6981(4)
b /Å	7.104(4)	7.198(2)	7.1667(2)	7.3191(3)	7.2936(1)
c /Å	3.779(2)	3.700(2)	3.5890(1)	3.7708(11)	3.7359(4)
α /°	95.98(4)	90	90	90	90
ß /°	90	95.85(4)	92.474(3)	90	90
γ /°	90	90	90	90	90
V /Å^3	686.48(4)	705.8(4)	679.71(1)	740.92(6)	727.48(2)
Z, Z'	2, 1/2	2, 1/2	2, 1/2	2, 1/2	2, 1/2
D_{calc} /Mg·m^{-3}	1.658	1.572	1.651	1.914	1.948
T /K	294	294	298	298	298
Radiation type	Cu *Kα*	Mo *Kα*	Cu $K\alpha_1$	Mo $K\alpha_1$	Cu $K\alpha_1$
Wavelength /Å	1.54178	0.71073	1.54056	0.70930	1.54056
θ_{max} /°	30	30	55	30	50
R_p /%			2.59	1.39	3.50
R_{wp} /%	6.39	6.37	3.56	1.89	4.60
R_{exp} /%			2.61	1.78	3.11
GOF			1.37	1.06	1.48
R_p' /% [c]			7.43	17.81	8.98
R_{wp}' /% [c]			9.04	13.06	10.24
R_{exp}' /% [c]			6.62	12.32	6.92
Pyridine stacking angle /° [d]	88.6	83.2	87.8	90	90

a) Unit cell transformed from the literature data with *a*' = *b*, *b*' = c, *c*' = *a* to correspond to the other structures.

b) Unit cell transformed from the literature data with *a*' = *a* + *c*, *b*' = *b*, *c*' = -*a* to correspond to the other structures.

c) *R*', R_{wp}' and R_p' values are background corrected according to the reference[28].

d) Angle between the pyridine ring mean plane and the stacking direction [001].

Table 3 Selected crystallographic data and Rietveld refinement parameters for compounds **1b** - **3b** and **5b**. In all structures the $[M(II)_2X_4]_n$ chains run along the ***c*** axis.

	α-1b (sample **1**)	**β-1b** (sample **3**)	**2b**	**3b**	**5b**
Compound	$[CuCl_2(4\text{-CNpy})]_n$	$[CuCl_2(4\text{-CNpy})]_n$	$[MnCl_2(4\text{-CNpy})]_n$	$[NiCl_2(4\text{-CNpy})]_n$	$[NiBr_2(4\text{-CNpy})]_n$
CCDC number	1535272	1535273	1535276	1535274	1535269
Ref.	This work	This work	This work	This work	This work
Structure determined from	Powder	Powder	Powder	Powder	Powder
Formula	$C_6H_4Cl_2CuN_2$	$C_6H_4Cl_2CuN_2$	$C_6H_4Cl_2MnN_2$	$C_6H_4Cl_2NiN_2$	$C_6H_4Br_2NiN_2$
MW /g·mol^{-1}	238.56	238.56	229.95	233.71	322.49
Crystal system	triclinic	monoclinic	monoclinic	monoclinic	monoclinic
Space group (No.)	$P\,\bar{1}$ (2)	$P\,1\,2_1/n\,1$ (14)	$P\,1\,1\,2/m$ (10)	$P\,1\,1\,m$ (6)	P 1 1 2/m (10)
a /Å	13.8312(3)	7.9609(4)	9.8938(6)	9.5049(3)	9.4827(2)
b /Å	7.9385(2)	27.3362(2)	12.0318(9)	7.5810(5)	12.3468(3)
c /Å	3.7907(5)	3.7947(2)	3.6493(2)	3.5132(1)	3.6898(5)
α /°	96.171(2)	90	90	90	90
ß /°	94.914(2)	97.482(2)	90	90	90
γ /°	96.825(2)	90	90.808(15)	128.019(4)	90.423(7)
V /Å^3	408.83(2)	818.76(7)	434.25(4)	199.43(2)	431.99(2)
Z, Z'	2, 1	4, 1	2, 1	1, 1	2, 1
D_{calc} /Mg·m^{-3}	1.938	1.935	1.758	1.947	2.480
T /K	298	298	298	298	298
Radiation type	Cu $K\alpha_1$	Cu $K\alpha_1$	Mo $K\alpha_1$	Cu $K\alpha_1$	Cu $K\alpha_1$
Wavelength /Å	1.54056	1.54056	0.70930	1.54056	1.54056
θ_{max} /°	55	55	40	55	50
R_p /%	3.35	4.28	3.01	3.35	3.55
R_{wp} /%	4.41	5.89	3.94	4.43	4.65
R_{exp} /%	2.53	2.82	2.10	2.99	2.86
GOF	1.74	2.09	1.88	1.49	1.63
R_p' /% [a]	9.49	13.24	11.23	10.76	9.65
R_{wp}' /% [a]	10.66	10.04	11.93	10.81	10.21
R_{exp}' /% [a]	6.12	7.19	6.35	7.28	6.27
Pyridine stacking angle /° [b]	86.4	84.5	90	90	90

a) *R'*, R_{wp}' and R_p' values are background corrected according to the reference[28].

b) Angle between pyridine ring mean plane and the stacking direction [001].

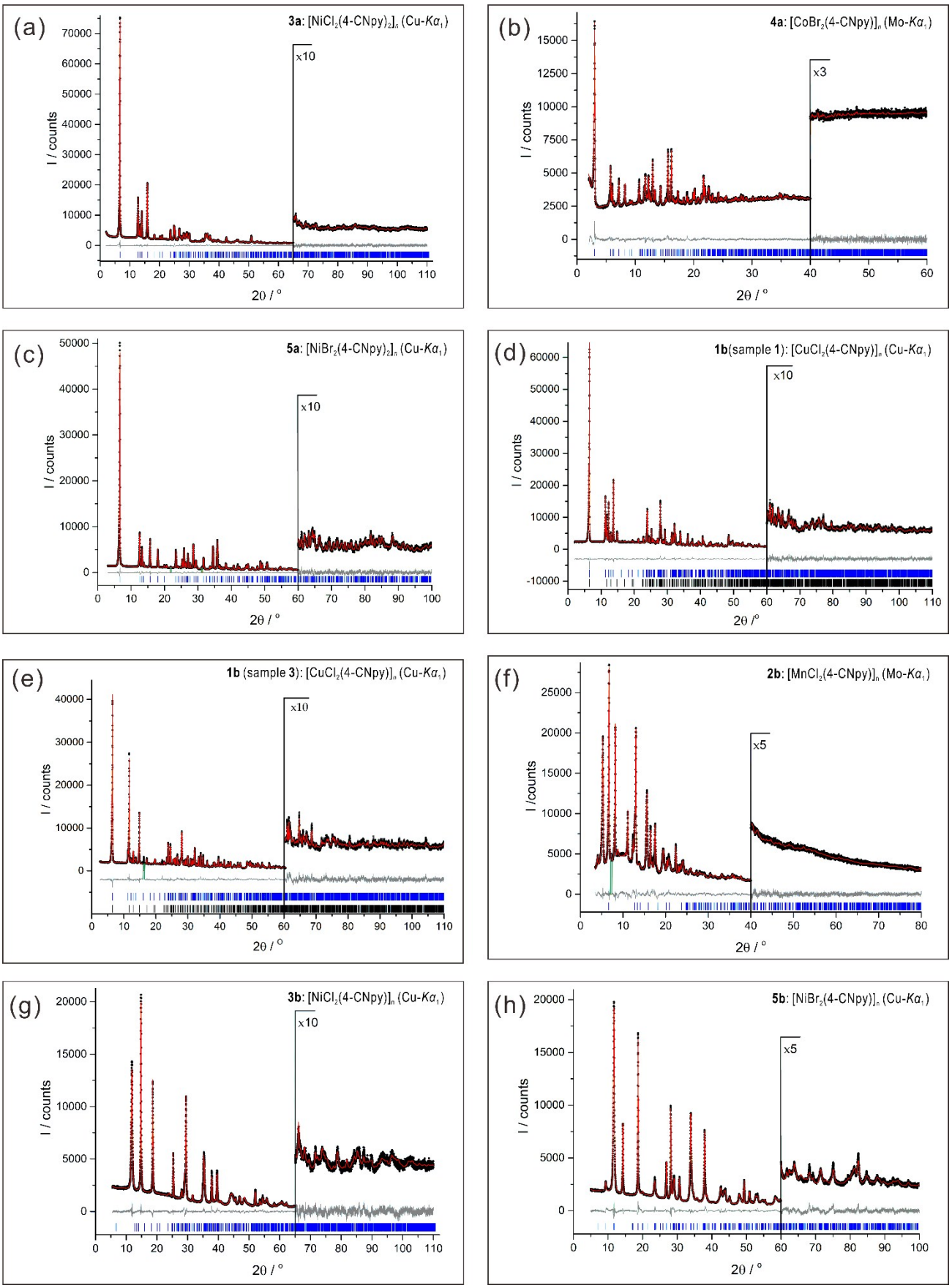

Fig. 4 Rietveld plots of **1b** - **3b**, **5b**, and **3a** - **5a**. Observed powder diagram (black points), simulated powder diagram (red solid line), difference profile (grey solid line), and reflection positions (blue tick marks, black for **β-1b**). Change of the scales with corresponding factors is remarked in the diagrams. Combined Rietveld refinements of **α-1b** and **β-1b** for sample **1** (d) and sample **3** (e). Excluded 2θ ranges are remarked by green lines (c, e, f).

Table 4 Selected bond distances between metal atoms and donor atoms. (*X* = Cl or Br)

	1a	2a	3a	4a	5a	α-1b	β-1b	2b	3b	5b
M(II)-N_{py} /Å	2 x 2.015(6)	2 x 2.286(8)	2 x 2.123(3)	2 x 2.202(9)	2 x 2.162(2)	2.001(7)	1.993(4)	2.311(8)	2.034(8)	2.185 (mean)
M(II)-*X*(1) /Å	2 x 2.957(3)	2 x 2.526(3)	2 x 2.437(2)	4x 2.617(4)	4 x 2.588(1)	2.295(3)	2.284(4)	2 x 2.565(6)	2 x 2.415(5)	2 x 2.561(3)
M(II)- *X*(2) /Å						2.302(4)	2.301(4)			
M(II)- *X*(3) /Å	2 x 2.276(3)	2 x 2.555(3)	2 x 2.123(3)			2.360(5)	2.311(4)	2 x 2.581(6)	2 x 2.436(4)	2 x 2.570(3)
M(II)- *X*(4) /Å						2.742(4)	2.569(4)			
M(II)- *X*(5) /Å						3.126(4)	3.225(4)			
M(II)-N_{CN} /Å								2.349(10)	2.079(6)	1.990 (mean)

Crystal structures

General

In all the crystal structures the *M*(II) atoms are octahedrally coordinated by 4 halogen and 2 nitrogen atoms (N_{py} and N_{CN}) or 5 halogen and 1 nitrogen atoms (N_{py}). Neighbouring octahedra are connected, in a first instance, by two μ_2-bridging halogen atoms each, resulting in a linear $[M(II)_2X_4]_n$ chain of edge-sharing octahedra. Within these chains, the metal-metal distances range from 3.51 Å (for **3b**) to 3.79 Å (for **1b**). Since the $[M(II)_2X_4]_n$ chains are running parallel in each structure, the metal-to-metal distance is the shortest translational periodicity in the structures, and accounts for a short lattice parameter *c* in all structures.

In the $[M(II)_2X_4]_n$ chains, the metal atoms are coordinated by four halogen atoms. The fifth coordination position of the octahedra is always occupied by a cyanopyridine ligand coordinating with its pyridine-nitrogen atom. Thereby the cyanopyridine ligands form lateral "wings" on one side of the $[M(II)_2X_4]_n$ chains.

For the sixth position at the metal coordination octahedra (*i.e.* in trans-position to the N atom), there are three possibilities:

(1) The position is filled by a second cyanopyridine ligand, also coordinating with its pyridine-nitrogen atom, resulting in single chains with a second wing at the other side of the $[M(II)_2X_4]_n$ chain (Scheme 1a, Fig. 5). This is the case for all compounds with a metal:ligand ratio of 1:2 (**1a - 5a**).

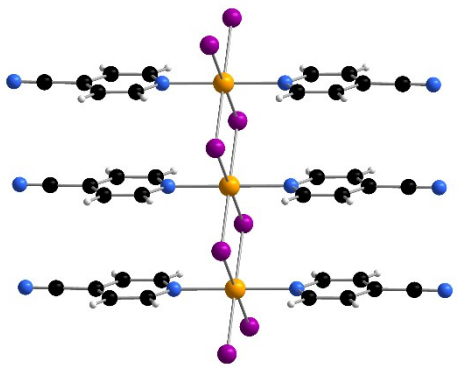

Fig. 5 Single chain of $[M(II)_2X_4]_n$ with lateral cyanopyridine 'wings' in the crystal structure of $[CoBr_2(4\text{-}CNpy)_2]_n$ (**4a**).

(2) The cyanopyridine ligand of a neighbouring chain coordinates with the N atom of the cyano group (Scheme 1c). Thereby the cyanopyridine acts as a linker between the two chains in compounds **2b**, **3b**, **4b** and **5b**.

(3) The sixth coordination position is filled by a Cl atom of a neighbouring $[M(II)_2X_4]_n$ chain, i.e. two $[M(II)_2X_4]_n$ chains aggregate via μ^3-Cl atoms into a double chain (Scheme 1b). This situation is found for both polymorphs of **1b**.

In the corresponding series of polymeric copper and nickel chloride complexes with unsubstituted pyridine as ligand, $[M(II)Cl_2(py)_x]_n$, case (1) is found for all compounds with $x = 2$, and case (3) for all compounds with $x = 1$[23,24]. For $x = 2/3$, triple chains are formed[23]. Phases with $x = 1/3$ were not observed. The phases of 4-cyanopyridine compounds with $x = 1/3$, $[MnCl_2(4\text{-}CNpy)_{1/3}]_n$ (**2c**) and $[CoBr_2(4\text{-}CNpy)_{1/3}]_n$ (**4c**) can be observed in the DTA/TG curves (Fig. 1b and Fig. S2), but could not be isolated. The stoichiometry would agree with a structure formed from triple chains connected by 4-cyanopyridine bridges.

The distances between the metal atoms and the coordinating atoms are compiled in Table 4. From the pronounced variation of the metal-halogen distances, it is evident that the copper compounds **1a**, **α-1b** and **β-1b**, and the nickel compounds **3a**, **5a** and **5b** exhibit a Jahn-Teller distortion of the octahedra.

In all structures, the pyridine rings of the cyanopyridine ligands have centre-to-centre distances, which are equivalent to the metal-metal-distances, i.e. 3.51 to 3.79 Å. This allows a good π···π stacking of the 4-cyanopyridine rings. In fact, neighbouring pyridine rings are always parallel to each other.

In **2b**, **3b**, **4a**, **5a** and **5b**, the pyridine rings are situated on mirror planes parallel to (001), hence the rings are exactly perpendicular to the stacking direction [001]. In contrast, the rings are not exactly perpendicular to the stacking direction in the other structures (**1a**, **2a**, **3a**, **1b**), with angles of 83.2° to 88.6° between the pyridine ring plane and the stacking direction. This inclination leads to a more efficient space filling and better van der Waals contacts. We cannot exclude that also in **2b**, **3b** and **4a** the pyridine rings are actually slightly inclined as well, and exhibit an orientational disorder across the mirror plane; such a disorder can hardly be detected from the powder diffraction data. But the small atomic displacement parameters indicate for the absence of such a

disorder. In all structures of $[M(II)X_2(4\text{-CNpy})_x]_n$ compounds all chains are parallel.

Structures built from single chains (1a - 5a)

All compounds $[M(II)X_2(4\text{-CNpy})_2]_n$ (**1a** - **5a**), having a metal:ligand ratio of 1:2, are built of linear $[M(II)_2X_4]_n$ single chains, which are equipped with two lateral cyanopyridine wings at each metal atom. The cyanopyridine ligands occupy the trans-positions of the octahedra. In all structures, the chains are arranged in a herringbone packing, see Fig. 6a and Fig. 7a. Neighbouring 'sheets' are shifted by 0.5 in the chain direction, to ensure a better van der Waals packing (Fig. 6b and Fig. 7b).

Although this herringbone arrangement is identical for the compounds **1a** - **5a**, there are small differences between the structures, caused by differences in the electronic structure of the metal atoms and the sites of the different halogen atoms. These differences become visible by viewing perpendicular to the chain direction. In the bromo compounds **4a** and **5a**, the pyridine rings are exactly perpendicular to the chain direction, leading to a crystallographic mirror plane (Fig. 7b). The angle β is 90°, the lattice is orthorhombic and the space group is *P* $2_1/n$ $2_1/n$ 2/*m*, with the Co atom occupying a 2/*m* site. The structure of **3a** is only pseudo-orthorhombic: All ligands are still co-planar, but the stacking direction is off the normal vector of the pyridine ring plane by 87.8° (Fig. 6b). The angle β changes from 90° to 92.47°, the lattice becomes monoclinic, and the space group is reduced to *P* 1 $2_1/n$ 1, which is a maximal "*translationengleiche*" subgroup of *P* $2_1/n$ $2_1/n$ 2/*m*. The Ni atom has a site symmetry of $\bar{1}$ only. Compounds **2a** and $[CoCl_2(4\text{-CNpy}]$[29] are isotopic to **3a**, but the inclination of the pyridine rings is even stronger (Fig. 8).

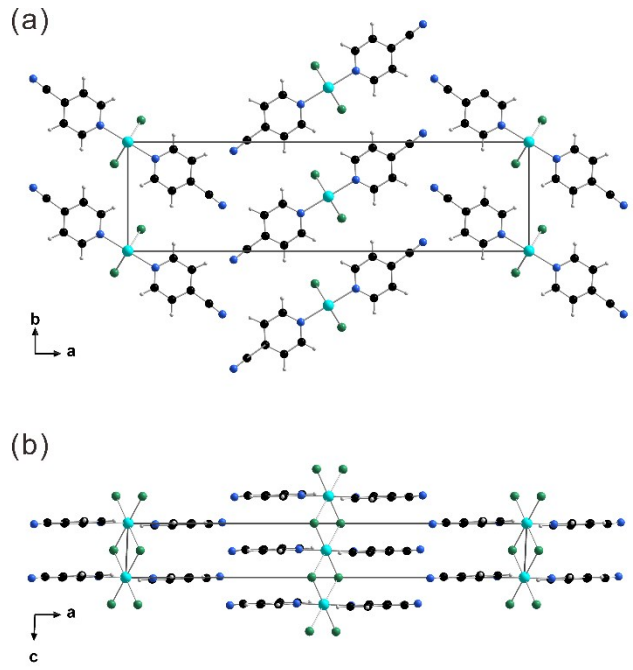

Fig. 6 Crystal structure of $[NiCl_2(4\text{-CNpy})_2]_n$ (**3a**). View along [00$\bar{1}$] (a) and [0$\bar{1}$0] (b).

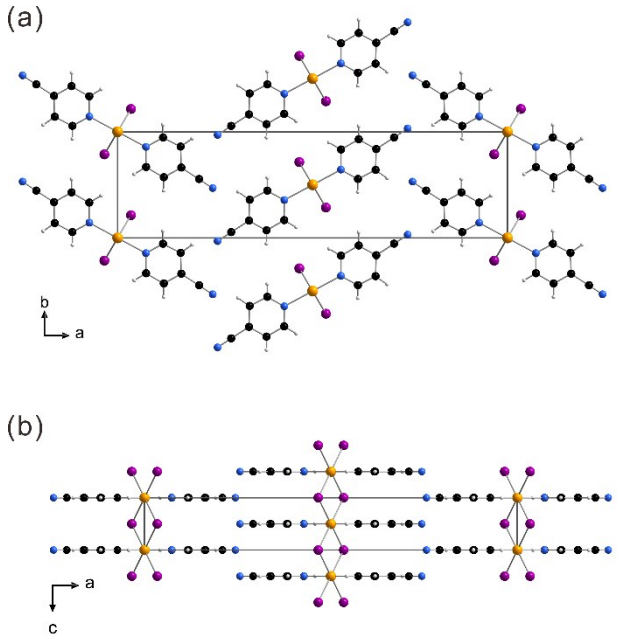

Fig. 7 Crystal structure of $[CoBr_2(4\text{-CNpy})_2]_n$ (**4a**). View along [00$\bar{1}$] (a) and [0$\bar{1}$0] (b).

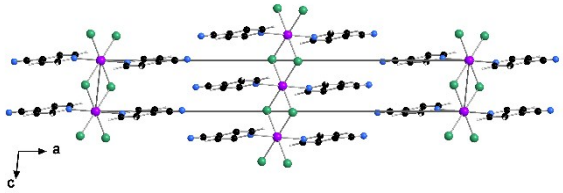

Fig. 8 Crystal structure of $[MnCl_2(4\text{-CNpy})_2]_n$ (**2a**). View along [0$\bar{1}$0].

In **1a**, the chains form a slight herringbone arrangement also when viewed from the side (Fig. 9). This leads to the space group *P* $2_1/n$ 1 1, which is another maximal "*translationengleiche*" subgroup of *P* $2_1/n$ $2_1/n$ 2/*m*. Note that *P* $2_1/n$ 1 1 (for **1a**) is different from *P* 1 $2_1/n$ 1 (for **2a** and **3a**): In **1a**, the monoclinic axis is the long axis (25.7 Å), but in **2a** and **3a**, it is the medium axis (7 Å).

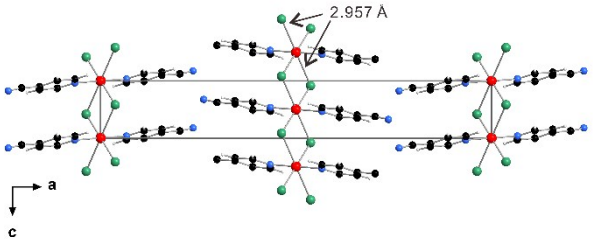

Fig. 9 Crystal structure of $[CuCl_2(4\text{-CNpy})_2]_n$ (**1a**). View along [0$\bar{1}$0]. Note: there are two strongly different Cu-Cl distances caused by Jahn-Teller distortion.

Structures with double chains (α-1b and β-1b)

For structures with a metal:ligand ratio of 1:1 there are two possibilities to fill the position of the missing ligand. Either a cyanopyridine of a neighbouring $[M(II)_2X_4]_n$ chain additionally coordinates with its cyano-nitrogen, thereby acting as a linker between the $[M(II)_2X_4]_n$ chains. Alternatively, two chains fuse into a double chain. Both possibilities were found in the compounds $[M(II)X_2(4\text{-CNpy})]_n$.

The copper compound $[CuCl_2(4\text{-CNpy})_2]_n$ (**1b**) is the only compound with a metal:ligand ratio of 1:1, which does not contain bridging 4-cyanopyridine units, but form double chains with lateral cyanopyridine "wings" at both sides. Obviously, the Cu (II) as d^9-ion is responsible for the resulting Jahn-Teller distortion and, therefore, for the occurrence of μ_3-Cl atoms, resulting in double chains instead of layers. As mentioned above, **1b** is polymorphic. The topology of the double chains is identical for both phases. The double chains, having the stoichiometry $[M(II)_2X_4]_n$, are formed by fusion of two single $[M(II)_2X_4]_n$ chains. Thereby two of the four chlorine atoms change from μ_2- to μ_3-bridging, *i.e.* they are connected to three different Cu atoms (Fig. 10). This leads to a double chain of edge-sharing octahedra (Fig. 10)

In both polymorphs, the coordination octahedra of Cu^{2+} show a remarkable Jahn-Teller distortion leading towards octahedra with two longer bonds in trans-positions. The three “equatorial” Cu-Cl bonds are quite short, with bond lengths between 2.295(3) and 2.360(5) Å for **α-1b** (and similar values for **β-1b**). The two 'axial' Cu-Cl distances are significantly longer, with values of 2.742(4) and 3.126(4) Å for **α-1b**, and 2.569(4) and 3.225(4) Å for **β-1b**. The Jahn-Teller effect is much stronger than the bond length difference between μ_2- and μ_3-coordinated chlorine ions: From the two Cu-Cl bonds of the μ_2-bridging chlorine atom, one is short, the other is long; from the three Cu-Cl bonds of the μ_3-connecting chlorine atoms, two are short, one is long (See Table 4). The two polymorphs of **1b** differ from each other in their arrangement of the $[M(II)_2X_4]_n$ chains. In the triclinic α-phase all double chains are parallel (Fig. 11), in contrast, a herringbone arrangement appears in the monoclinic phase (Fig. 12).

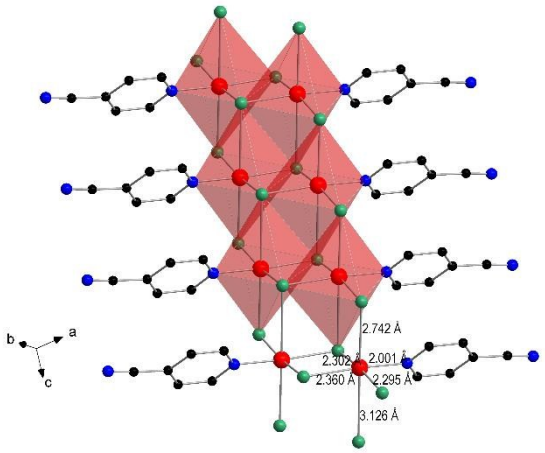

Fig. 10 Double chain $[M(II)_2X_4]_n$ of edge-sharing octahedra with adjecent ligands in the crystal structure of **α-1b** (H atoms omitted for clarity).

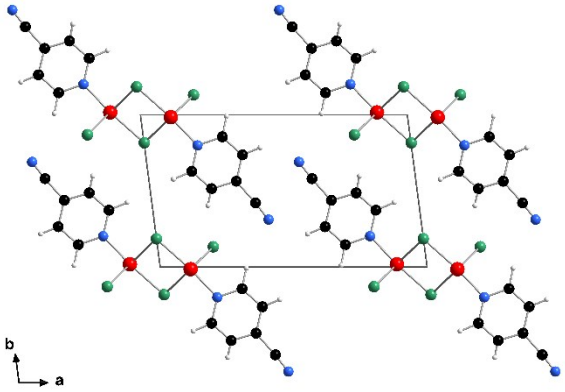

Fig. 11 Parallel arrangement of double chains in the crystal structure of **α-1b**. View along $[00\bar{1}]$

In both polymorphs, the cyanopyridine groups of neighbouring double chains show a vertical offset of *c*/2 to ensure a good van der Waals packing, see Fig. 13.

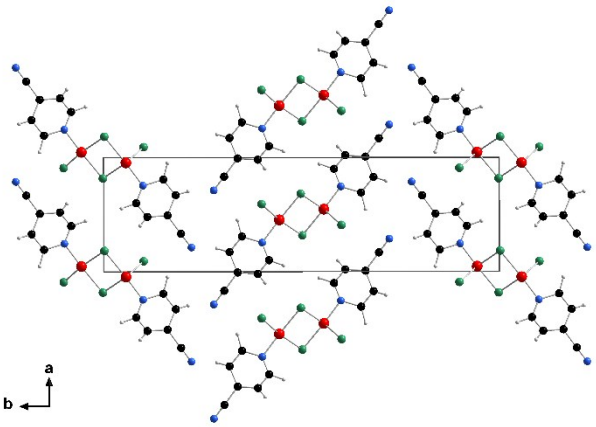

Fig. 12 Herringbone arrangement of double chains in the crystal structure of **β-1b**. View along $[00\bar{1}]$.

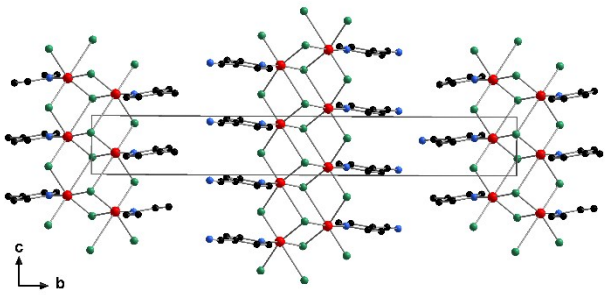

Fig. 13 Vertical arrangement of neighbouring chains in the crystal structure of **β-1b**. View along $[\bar{1}00]$. (H atoms omitted for clarity).

Structures with bridging cyanopyridine ligands (2b, 3b, 5b)

The crystal structures of $[MnCl_2(4\text{-CNpy})]_n$ (**2b**), $[NiCl_2(4\text{-CNpy})]_n$ (**3b**) and $[NiBr_2(4\text{-CNpy})]_n$ (**5b**), determined here, are the first crystal structures, where the 4-cyanopyridine acts as a linker between two 3d transitional metal atoms. The 4-cyanopyridine coordinates not only with the nitrogen atom of the pyridine ring, but also with its cyano nitrogen atom, as it was also revealed by the IR data.

The bridges between the $[M(II)_2X_4]_n$ chains lead to a layer parallel to (010), see Fig. 14. Each metal atom is coordinated from one 4-cyanopyridine ligand with its pyridine-nitrogen atom, a second one with its cyano group. The theoretically possible case of a metal atom surrounded either by two cyano groups or by two pyridine rings, is not observed. Within a layer, all cyanopyridine bridges have the same orientation. In the neighbouring layers, the orientation may be either inverted, or the orientation of the cyanopyridine can be the same in all layers.

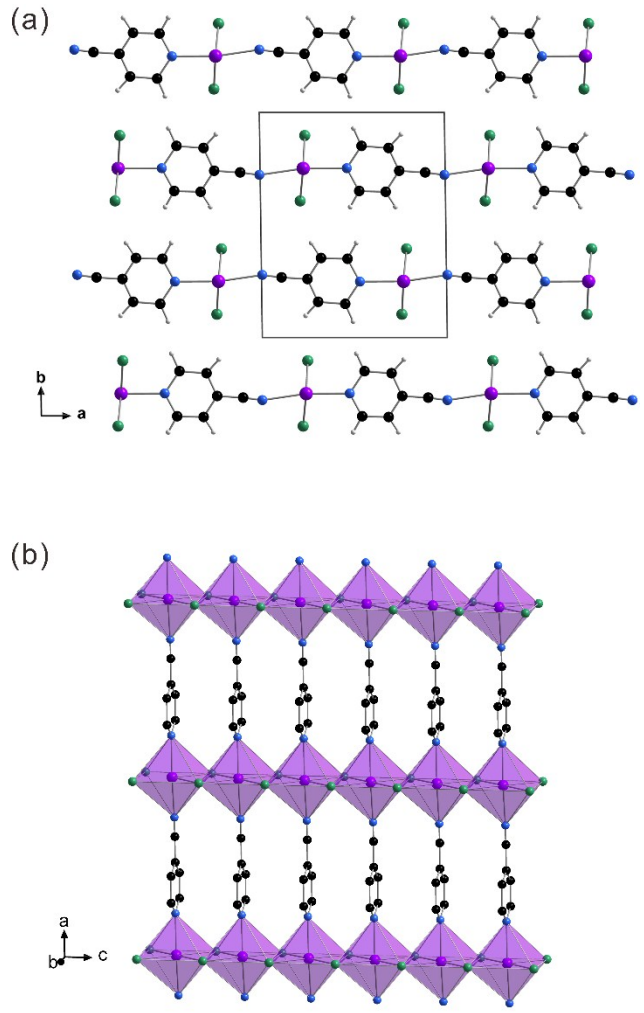

Fig. 14 Crystal structure of $[MnCl_2(4\text{-CNpy})]_n$ (**2b**). (a) View along $[00\bar{1}]$. (b) One single layer (H atoms omitted for clarity). All atoms are on vertical mirror planes parallel to (001).

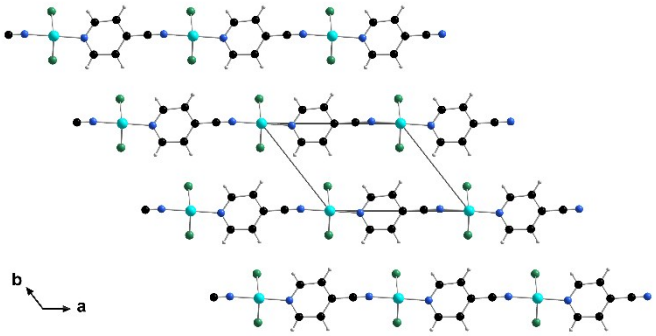

Fig. 15 Crystal structure of $[NiCl_2(4\text{-CNpy})]_n$ (**3b**). View along $[00\bar{1}]$.

The former case leads to the non-polar crystal structure of **2b** in space group *P* 1 1 2/*m*, with all atoms on mirror planes parallel to (001) (Fig. 14a). The structure is pseodo-orthorhombic, with a monoclinic angle of 90.81(2)° only. The orthorhombic space group would be *P* 2/*b* 2_1/*m* 2/*m*, which is a non-standard setting of *Pmma*. In this space group, Ni and N atoms would be situated on sites with 2*mm* symmetry. The main deviation from the orthorhombic symmetry is that the $[M(II)_2X_4]_n$ chain is not exactly parallel to the (100) plane, but forms an angle of 6.0° with it.

In the crystal structure of **3b** (Fig. 15 and Fig. S5), all cyanopyridine fragments have an identical orientation. This leads to the polar structure of **3b** in the space group *P* 1 1 *m*, *Z* = 1, with all cyanopyridine rings being exactly parallel. Here, all atoms are situated on crystallographic mirror planes.

The *M*(II)–(4-CNpy)–*M*(II) fragments are not exactly linear, but show a slight zig-zag shape. The cyano group exhibits a C≡N-*M*(II) angle of 171.5° for **2b**, 176.7 for **3b** and 172.0° for **5b**. These values are in good agreement with the C≡N-*M*(II) angle in the known single-crystal structures: 176.9° for 178.1 for $[Ag(4\text{-CNpy})]_n(nBF_3)$[19]. However, the C≡N-Cd angle is even stronger bended in other structures, with an C≡N-Cd angle of 148.7°, in the single-crystal structure of $[Cd(SCN)_2(4\text{-CNpy})]_n$[21].

In **3b**, the Ni(II) coordination octahedra are slightly contracted in comparison to the Mn(II) octahedra of **2b**. Furthermore, a significant Jahn-Teller distortion is visible for the nickel compound (**3b**): The mean *M*(II)-N distances decrease from 2.33 Å for the manganese compound to 2.08 Å for the nickel compound, whereas the *M*(II)-Cl distances decrease only by 0.15 Å.

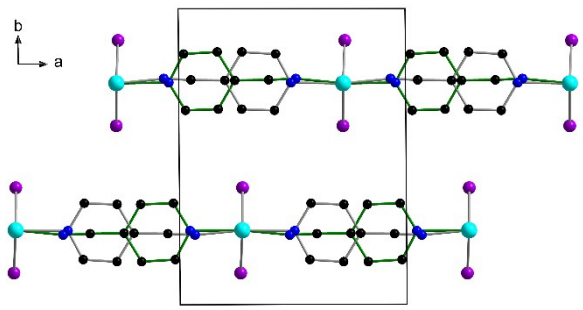

Fig. 16 Head-to-tail disorder of the 4-cyanopyridine ligands in the crystal structure of **5b**. View along $[00\bar{1}]$. (H atoms omitted for clarity)

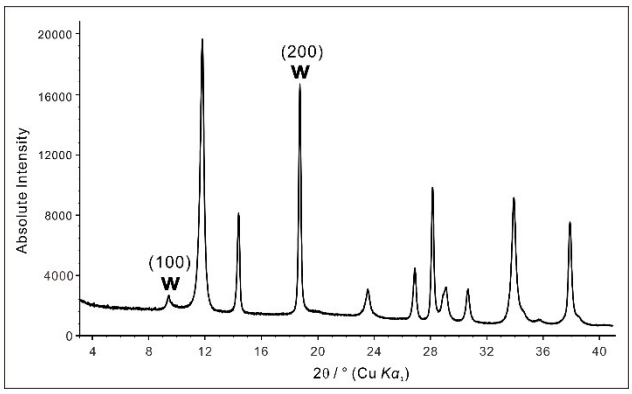

Fig. 17 Low-range part of powder pattern of **5b**. The Warren peaks (100) and (200) are marked by "W".

In the crystal structure of $[NiBr_2(4\text{-}CNpy)_2]_n$ (**5b**), the arrangement of the layers is the same as in **2b**. However, the cyanopyridine bridges of **5b** show a head-to-tail-disorder with two molecular orientations (Fig. 16). In both orientations, both nitrogen atoms bind to the nickel atoms, but the carbon (and hydrogen) atoms swap their positions. The occupancies for the two orientations are 0.468 (green marked 4-cyanopyridine in Fig. 16) and 0.532. From the powder data themselves, it is not evident, if the cyanopyridine groups within one layer are disordered, or if the disorder concerns orientational disorder of ordered layers. In all cases, the disorder causes diffuse scattering. In the powder diagram of **5b**, this diffuse scattering is visible as Warren peaks, *i.e.* peaks with tails towards higher diffraction angles, especially pronounced for the marked reflections (see Fig. 17).

For **2b** and **3b**, a head-to-tail disorder cannot be completely excluded, but the the Rietveld refinements with a disorder model reveal that the occupancy of the second molecular orientation must be lower than 10%. Also two of the four literature structures of 4d metals with bridging 4-cyanopyridine rings show this head-to-tail disorder of the cyanopyridine fragment: The complexes with Ru[17] and Rh[18] are disordered, whereas the structures with Ag[19,20] and Cd[21] are ordered.

Conclusions

This work has shown that 4-cyanopyridine can be used as a versatile ligand. The new compounds $[MnCl_2(4\text{-}CNpy)]_n$ (**2b**), $[NiCl_2(4\text{-}CNpy)]_n$ (**3b**) and $[NiBr_2(4\text{-}CNpy)]_n$ (**5b**) are the first known compounds where 4-cyanopyridine acts as a linker between two 3d transitional metal atoms (Mn, Ni).

The choice, whether 4-cyanopyridine acts as a bidentate or a as monodentate ligand depends on the metal (II) atom, the halogen atom and the stoichiometric metal:ligand ratio. All 1:2 compounds of the type $[M(II)X_2(4\text{-}CNpy)_2]_n$ with Mn, Co, Ni or Cu, and X = Cl or Br (**1a**-**5a**), exhibit a monodentate behaviour of the ligand which results in linear polymeric $[M(II)_2X_4]_n$ single chains built by edge-sharing octahedra. The ligands are attached as lateral 'wings' on both sides of the chains. The chains are arranged in a herringbone packing. The structural differences between the five compounds **1a-5a** are small, but lead to four different structures in three different space groups.

For the 1:1 compounds $[M(II)X_2(4\text{-}CNpy)]_n$, two different structure types are observed: a) two-dimensional networks, in which the $[M(II)_2X_4]_n$ chains are connected through bridging 4-cyanopyridine linkers, which coordinate the M(II) atoms additionally by their N_{CN} atoms; b) polymeric double chains, which emerge by fusing two $[M(II)_2X_4]_n$ chains through μ_3-Cl atoms. For the copper compound $[CuCl_2(4\text{-}CNpy)]_n$ (**1b**), we found the double chains, whereas for all other compounds ($[MnCl_2(4\text{-}CNpy)]_n$ (**2b**), $[NiCl_2(4\text{-}CNpy)]_n$ (**3b**) and $[NiBr_2(4\text{-}CNpy)]_n$ (**5b**)), we observed the intended formation of two-dimensional networks with 4-cyanopyridine bridges between the metal atoms.

The topology of the networks of **2b** and **3b** is identical, however the arrangement is different: In **2b**, the layers are stacked in an anti-parallel orientation to each other. For **3b**, we found an arrangement of parallel layers leading to a polar structure with space group *P* 1 1 *m*. Therefore, **3b** may own optical activity, pyroelectricity, piezoelectricity and second-harmonic generation. The crystal structure of **5b** shows an interesting head-to-tail disorder of the 4-cyanopyridine groups with a distribution of about 4:6 for the two orientations of the ligand.

The copper compound $[CuCl_2(4\text{-}CNpy)]_n$ is the only 1:1 compound, in which the 4-cyanopyridine acts as a monodentate ligand. The compound is polymorphic. In both phases, the Cu(II) atoms, having a d^9 configuration, show a strong Jahn-Teller distortion of the octahedra with Cu-Cl bond lengths varying from 2.28 to 3.26 Å. We found the monodentate behaviour of the organic ligand due to the d^9-configuration of the copper, causing Jahn-Teller distortion of the coordination octahedra in **1b**. The two polymorphic phases of **1b** differ by the arrangement of the double chains, which can be either parallel (**α-1b**) or in a herringbone pattern (**β-1b**). The formation of the different polymorphs depends on the synthetic conditions, especially on the temperature profiles. Temperature-dependent XRPD should in future be made on the other coordination polymers, too, in order to investigate a possible polymorphism as well.

With 4-cyanopyridine as a ligand, a spectrum of various coordination chemistry is available. One-dimensional single chains or double chains and two-dimensional networks are realized. The degree of polymerization can be tuned by thermal decomposition from chains to double chains and 2D networks. By further increase of the metal:ligand ratio or a variation of the counterions, even new three-dimensional frameworks (e.g. MOFs) should be conceivable.

Experimental section

Materials

Methanol, ethanol and 4-cyanopyridine were purchased from Sigma-Aldrich. $MnCl_2{\cdot}4H_2O$, $NiCl_2{\cdot}6H_2O$ and $CuCl_2{\cdot}2H_2O$ were obtained from Fluka. $CoBr_2$ and $NiBr_2$ were purchased from Alfa Aesar.

Syntheses of $[CuCl_2(4\text{-}CNpy)_2]_n$ (1a)

$CuCl_2 \cdot 2H_2O$ was dried at 100 °C for 120 minutes. Anhydrous $CuCl_2$ (1.983 g, 14.75 mmol) was dissolved in 60 mL of methanol. The solution was dropwise added by a 60 mL methanol solution of 4-cyanopridine (3.07 g, 29.5 mmol). After a constant stirring for 90 minutes the mixture was filtered off and washed with methanol. The final residue was dried in a vacuum desiccator (drying agent: silica gel) for one night to get **1a** as a light blue powder. The compound was identified by X-ray powder diffraction data comparing with calculated powder pattern. Yield: 4.683 g (92.26%). IR (cm^{-1}): *v* 2242(w), 1611(s), 1551(m), 1494(m), 1415(s), 1219(s), 1065(m), 1027(m), 829(s), 785(m) (Fig. S6).

Preparation of $[CuCl_2(4\text{-}CNpy)]_n$ (1b)

Compound **1b** was prepared by thermal decomposition reaction of **1a**. sample **1** of **1b** was prepared in a glass capillary on a STOE Stadi-P diffractometer equipped with a heating device which gives a hot nitrogen flow (about 220°C). The other samples were obtained from the thermal decomposition in a snap cap vial in a tube furnace under nitrogen atmosphere at 207 °C for 150 minutes (sample **2**) and at 220 °C for 120 minutes (sample **3**) respectively. Schematic representation for preparations of samples **2** and **3** can be found in the supporting information (Fig. S7). Yield: 99.96% for sample **2** and 94.94% for sample **3**. IR of sample **2** (cm^{-1}): 3102(w), 3058(w), 3012(w), 2243(w), 1698(w), 1612(m), 1497(w), 1417(s), 1219(m), 1067(w), 1029(w), 834(s), 785(w), 671 (w) (Fig. S8).

Syntheses of $[MnCl_2(4\text{-}CNpy)_2]_n$ (2a)

$MnCl_2 \cdot 4H_2O$ was dried at 100 °C for 120 minutes. Anhydrous $MnCl_2$ (1.346 g, 10.7 mmol) was dissolved in 50 mL ethanol. A 50 mL ethanol solution of 4-cyanopridine (2.227 g, 21.38 mmol) was mixed with the prepared $MnCl_2$/methanol solution. The mixture was stirred for 90 minutes at room temperature. The precipitate was isolated by filtration and washed with ethanol. The final residue was dried in a vacuum desiccator (drying agent: silica gel) for one night to give white powder. It was identified by X-ray powder diffraction data comparing with calculated powder pattern. Yield: 2.821g (78.95%). IR (cm^{-1}): 3096(w), 3051(w), 2241(w), 1606(s), 1550(m), 1494(m), 1413(s), 1226(s), 1216(m), 1194(w), 1065(s), 1011(s), 826(s), 789(s) (Fig. S9).

Preparation of $[MnCl_2(4\text{-}CNpy)]_n$ (2b)

Compound **2b** was prepared by thermal decomposition reaction of $[MnCl_2(4\text{-}CNpy)_2]_n$. $[MnCl_2(4\text{-}CNpy)_2]_n$ (0.1432 g, 0.429 mmol) was filled in a snap cap vial and heated in a muffle furnace at 220 °C for 120 minutes. After cooling a white crystalline powder (0.0976 g, 0.424 mmol) was obtained. Yield: 99.02 %. IR (cm^{-1}): 3093(w), 3070(w), 2275(w), 1603(m), 1550(w), 1490(w), 1411(s), 1215(m), 1067(w), 1012(w), 959(w), 821(s), 799(s) (Fig. S10).

Syntheses of $[NiCl_2(4\text{-}CNpy)_2]_n$ (3a)

Compound **3a** was synthesized similar to the synthesis of $[MnCl_2(4\text{-}CNpy)_2]_n$. A light green crystalline product was obtained by a reaction of nickel chloride hexahydrate (2.347 g, 9.87 mmol) and cyanopyridine (2.056g, 19.75 mmol) in ethanol for 90 minutes. Yield: 2.958 g (88.68%). IR (cm^{-1}): 3105(w), 2242(w), 1610(s), 1551(m), 1492(m), 1414(s), 1220(s), 1066(m), 1020(m), 821(s), 782(m) (Fig. S11).

Preparation of $[NiCl_2(4\text{-}CNpy)]_n$ (3b)

Compound **3b** was prepared by thermal decomposition reaction of **3a**. Compound **3a** (0.2261 g, 0.669 mmol) was filled in a snap cap vial and heated in a muffle furnace at 220 °C for 180 minutes. After cooling a light blue residue (0.1564 g, 0.669 mmol) was obtained. Yield: 99.98 %. IR (cm^{-1}): 3176(w), 2288(w), 1605(m), 1551(w), 1490(w), 1411(s), 1215(s), 1067(w), 1019(w), 821(s), 792(m) (Fig. S12).

Synthesis of $[CoBr_2(4\text{-}CNpy)_2]_n$ (4a)

Anhydrous Cobalt bromide (0.53 g, 2.4 mmol) was dissolved in 8 mL ethanol, 4-cyanopyridine (0.55 g, 5.3 mmol) was dissolved in 5 mL ethanol. Both solutions were stirred, heated up to 70 °C and mixed to form a violet precipitate. After stirring for an additional hour, the slurry was cooled to room temperature, filtrated and washed three times with 5 mL ethanol. The final residue was dried in air for 1 h and overnight in a desiccator (drying agent: silica gel). The product (yield: 0.99 g, 2.3 mmol, 96 %) was characterized by thermal analysis IR and X-ray powder diffraction data. IR(cm^{-1}): 3102(w), 3056(w), 2234(w), 1606(s), 1547(m), 1487(m), 1408(s), 1209(s), 1187(m), 1058(s), 1016(s), 819(s), 776(s), 674(m) (Fig. S13).

Synthesis of $[CoBr_2(4\text{-}CNpy)]_n$ (4b)

A evacuated and sealed glas ampule, equipped with a well distributed 1:1 molar mixture of $CoBr_2$ (0.12 g, 0.55 mmol) and **4a** (0.23 g, 0.54 mmo), was placed in a tube furnance with temperature gradient (maximum temperature 360 °C) for 22 h. After cooling down within 4 h different phases of $[CoBr_2(4\text{-}CNpy)_x]_n$ (x = 0 - 2), ranging from **4a** to pure $CoBr_2$ were obtained (Fig. S14). Fraction **2**, $[CoBr_2(4\text{-}CNpy)]_n$ (**4b**), was isolated as grey powder of poor crystallinity. IR(cm^{-1}): 3096(w), 3072(w), 3046(w), 2281(w), 1605(m), 1549(m), 1496(w), 1409(s), 1216(s), 1096(m), 1063(s), 1015(s), 819(s), 787(m), 671(w), 560(s), 458(w) (Fig. S15).

Synthesis of $[NiBr_2(4\text{-}CNpy)_2]_n$ (5a)

Anhydrous Nickel bromide (0.25 g, 2.29 mmol) was dissolved in 35 mL 4-Hydroxy-4-methylpentan-2-one (DAA), 4-cyanopyridine (0.477 g, 9.16 mmol) was dissolved in 10 mL DAA. Both solutions were mixed and put in a fridge at 8°C. A light yellow powder was formed after 3 days. The powder was washed four times with 2 mL methanol and dried overnight in a desiccator (drying agent: silica gel). The product was characterized by thermal analysis, X-ray powder diffraction data and IR (cm^{-1}): 3105(w), 2235(w), 1607(s), 1549(m), 1489(m), 1412(s), 1219(s), 1196(m), 1063(s), 1018(s), 816(s), 783(s), 675(m) (Fig. S16).

Preparation of $[NiBr_2(4\text{-}CNpy)]_n$ (5b)

Compound **5b** was prepared by thermal decomposition reaction of **5a**. Compound **5a** (0.02216 g, 0.0520mmol) was heated in a thermogravimetric device (details see below) at 280 °C for 10 minutes under Argon atmosphere. After cooling an ochre powder (0.01712 g) was obtained and immediately transferred into a glass capillary. The capillary was sealed and put on the diffractometer. The product was characterized by X-ray powder diffraction data and IR (cm^{-1}): 3310(w), 3229(w) 2298(w), 1630(m), 1551(w), 1418(s), 1217(s), 1067(w), 1024(w), 831(s), 820(s), 783(m) (Fig. S17).

Spectroscopy

FT-IR spectra were recorded with a NICOLET 6700 Fourier Transform Infrared Reflection–Absorption Spectrometer.

Differential thermal analysis and thermogravimetry (DTA/TG)

Differential thermal and thermogravimetric analysis (DTA/TG) were performed on a SETARAM (TGA 92) device. The samples were filled into Al_2O_3 crucibles and measured under nitrogen atmosphere with a heating rate of 5 K/min and a constant flow rate of about 75 mL/min. The heating ranges for the compounds are from 293 K to 873 K for $[MnCl_2(4\text{-}CNpy)_2]_n$, from 293 K to 713 K for $[NiCl_2(4\text{-}CNpy)_2]_n$ and from 293 K to 723 K for $[CuCl_2(4\text{-}CNpy)_2]_n$.

X-ray powder diffraction

For the crystal structure determination from X-ray powder diffraction data, the XRPD experiments were performed on a STOE Stadi-P diffractometer equipped with a Ge(111) monochromator and a linear position-sensitive detector (PSD) using Cu $K\alpha_1$ radiation (λ = 1.54056 Å) for **1b**, **3a**, **3b, 5a, 5b** and Mo $K\alpha_1$ radiation (λ = 0.70930 Å) for **2b**, **4a**. The specimens were measured in borosilicate glass capillaries with a diameter of 1.0 mm for **1b**, **3a**, **3b, 5a, 5b** and 0.5 mm for **2b**, **4a**. The data was collected with *WinXPOW* software[30].

The temperature dependent XRPD measurement for compound **1a** was performed on a STOE Stadi-P diffractometer equipped with a ceramic oven and an imaging plate position-sensitive detector using Cu $K\alpha_1$ radiation. The measurements were carried out in a 1.0 mm glass capillary under static air.

Structure determinations from X-ray powder data

General

All the powder patterns were indexed with DICVOL91[31]. The space group determination was carried out in DASH[32]. All structures were solved with a starting molecular structure model in direct space using simulated annealing in DASH. Rietveld refinements were performed with TOPAS[28]. First, a Pawley refinement was carried out to refine background, zero point error, unit cell parameters, peak width and peak asymmetry parameters. In the Rietveld refinements, the cyanopyridine ring including H atoms was restrained to be flat; the bond lengths and bond angles in the pyridine ring and the cyano group were restrained to a statistical mean value from Cambridge structural database (CSD) (Fig. S18 and Table S3). The values of isotropic thermal parameters of H atoms were constrained to be 1.2 times of those of the non-hydrogen atoms.

$[CuCl_2(4\text{-}CNpy)]_n$ (α-1b and β-1b)

The samples of **1b**, measured carefully at room temperature, contained always a mixture of the α- and the β-phase. The powder pattern of **α-1b** could be obtained by subtracting the pattern of sample **2** from that of sample **1**; the pattern of **β-1b** by subtracting the patterns of sample **3** and sample **2**. For the β-phase of **1b**, the indexing of extracted X-ray powder pattern with 21 peaks led to a monoclinic unit cell with ($M(21)$ = 24.9; $F(21)$ = 49.6). A comparison of the unit cell volume (814.2 $Å^3$) with Hofmann's volume increments[33] indicated for Z = 4. The same molecular structure model as **1a** was applied in the structure solution.

For **α-1b**, a total of 21 peaks in the low angle range were selected for indexing of the extracted X-ray powder of the pure phase. The indexing led to a triclinic unit cell with a figure of merit[34,35] ($M(21)$ = 14.0; $F(21)$ = 24.9). A comparison of the unit cell volume from indexing (406.4 $Å^3$) with Hofmann's volume increments led to Z = 2. The starting molecular geometry for structure solution of **α-1b** was constructed from the known crystal structure of $[CuCl_2(4\text{-}CNpy)_2]_n$.

Rietveld refinements were performed on the original data of sample **1**, refining the structures of both phases simultaneously (Fig. 4d and 4e). The same procedure was also applied to sample **2** (Figs S4). The resulting crystal structures were virtually identical. R-values and relative amounts of both phases are given in Table S2. The highest content of **α-1b** was found in sample **1** (72%), and the highest amount of **β-1b** in sample **3** (86%). Correspondingly, the final crystallographic data of **α-1b** were taken from the Rietveld refinement of sample **1**, that of **β-1b** from the refinement of sample **3**.

$[MnCl_2(4\text{-}CNpy)]_n$ (2b)

Indexing with the first 20 peaks led a monoclinic unit cell. A starting molecular geometry was generated from the known crystal structure of $[MnCl_2(4\text{-}CNpy)_2]_n$[24]. Due to the slight residue of compound **2a** the 2θ range from 7.1° to 7.4° was excluded in Rietveld refinement.

$[NiCl_2(4\text{-}CNpy)_2]_n$ (3b)

The first 28 peaks were selected for indexing, which resulted in a monoclinic unit cell. The starting molecular geometry was derived from the known crystal structure of $[MnCl_2(4\text{-}CNpy)_2]_n$, in which the Mn atom was replaced by Ni.

$[NiCl_2(4\text{-}CNpy)]_n$ (3a)

Indexing with 19 low-angle peaks led to a monoclinic unit cell. The molecular structure model was derived from the previously determined crystal structure of **3b**.

$[CoBr_2(4\text{-}CNpy)_2]_n$ (4a)

Indexing of the X-ray powder pattern led to an orthorhombic unit cell. A starting molecular geometry was generated from the known crystal structure of compound **3b** and force field methods in AVOGADRO[36].

$[NiBr_2(4\text{-}CNpy)_2]_n$ (5a)

Indexing with 19 low-angle peaks led to an orthorhombic unit cell. The molecular structure model was derived from the previously determined crystal structure of **4a**. Due to the slight residue of a decomposition intermediate of **5b**, the 2θ ranges from 21.7° to 22.0° and 31.0° to 31.3° were excluded in Rietveld refinement.

$[NiBr_2(4\text{-}CNpy)]_n$ (5b)

Indexing with 21 low-angle peaks led to a monoclinic unit cell. The molecular structure model was derived from the previously determined crystal structure of **5a.**

Acknowledgements

Haishuang Zhao gratefully acknowledges financial support by the Carl-Zeiss-Stiftung.

References

1 T. Watabe and K. Yogo, *Bull. Chem. Soc. Jpn.*, 2014, **87**, 740–745.
2 J. Hasegawa, M. Higuchi, Y. Hijikata and S. Kitagawa, *Chem. Mater.*, 2009, **21**, 1829–1833.
3 Z. Wang, G. Chen and K. Ding, *Chem. Rev.*, 2008, **109**, 322–359.
4 S.-H. Cho, B. Ma, S. T. Nguyen, J. T. Hupp and T. E. Albrecht-Schmitt, *Chem. Commun.*, 2006, 2563–2565.
5 O. R. Evans and W. Lin, *Acc. Chem. Res.*, 2002, **35**, 511–522.
6 S. Wöhlert, L. Fink, M. Schmidt and C. Näther, *CrystEngComm*, 2013, **15**, 945–957.
7 Y.-S. Bae, O. K. Farha, A. M. Spokoyny, C. A. Mirkin, J. T. Hupp and R. Q. Snurr, *Chem. Commun.*, 2008, 4135–4137.
8 M. Wriedt, S. Sellmer and C. Näther, *Dalton Trans.*, 2009, 7975–7984.
9 J. Lee, O. K. Farha, J. Roberts, K. A. Scheidt, S. T. Nguyen and J. T. Hupp, *Chem. Soc. Rev.*, 2009, **38**, 1450–1459.
10 S. L. James, *Chem. Soc. Rev.*, 2003, **32**, 276–288.
11 F. H. Allen, *Acta Crystallogr. B*, 2002, **58**, 380–388.
12 I. J. Bruno, J. C. Cole, P. R. Edgington, M. Kessler, C. F. Macrae, P. McCabe, J. Pearson and R. Taylor, *Acta Crystallogr. B*, 2002, **58**, 389–397.
13 D. T. Cromer and A. C. Larson, *Acta Crystallogr. B*, 1972, **28**, 1052–1058.
14 A. J. Graham, P. C. Healy, J. D. Kildea and A. H. White, *Aust. J. Chem.*, 989, **42**, 177–184.
15 M. K. Broderick, C. Yang, R. D. Pike, A. Nicholas, D. May and H. H. Patterson, *Polyhedron*, 2016, **114**, 333–343.
16 H. Hanika-Heidl, S. E. H. Etaiw, M. S. Ibrahim, A. S. B. El-din and R. D. Fischer, *J. Organomet. Chem.*, 2003, **684**.
17 A. Bacchi, G. Cantoni, P. Pelagatti and S. Rizzato, *J. Organomet. Chem.*, 2012, **714**, 81–87.
18 W. H. Leung, W. Lai and I. D. Williams, *J. Organomet. Chem.*, 2000, **604**, 197–201.
19 L. Carlucci, G. Ciani, D. M. Proserpio and A. Sironi, *J. Chem. Soc., Chem. Commun.*, 1994, 2755–2756.
20 X. L. Zhao and T. C. W. Mak, *Dalton Trans.*, 2004, 3212–3217.
21 W. Chen, F. Liu and X. You, *Bull. Chem. Soc. Jpn.*, 2002, **75**, 1559–1560.
22 R. D. Bailey and W. T. Pennington, *Chem. Commun.*, 1998, 1181–1182.
23 Y. Krysiak, L. Fink, T. Bernert, J. Glinnemann, M. Kapuscinski, H. Zhao, E. Alig and M. U. Schmidt, *Z Anorg Allg Chem*, 2014, **640**, 3190–3196.
24 W. Zhang, J. R. Jeitler, M. M. Turnbull, C. P. Landee, M. Wei and R. D. Willett, *Inorganica Chim. Acta*, 1997, **256**, 183–198.
25 M. L. Hernández, M. G. Barandika, M. K. Urtiaga, R. Cortés, L. Lezama, M. I. Arriortua and T. Rojo, *J. Chem. Soc. Dalton Trans.*, 1999, 1401–1406.
26 S. Wöhlert, I. Jess, U. Englert and C. Näther, *CrystEngComm*, 2013, **15**, 5326–5336.
27 S. Wöhlert, L. Fink, M. U. Schmidt and C. Näther, *Z Anorg Allg Chem*, 2013, **639**, 2186–2194.
28 A. Coelho, *TOPAS Acad. User Man. & Tech. Ref.*, 2009, Brisbane, Australia.
29 W. T. Chen, Z. G. Luo, Y. P. Xu, Q. Y. Luo and J. H. Liu, *J. Chem. Res.*, 2011, **35**, 253–256.
30 STOE & Cie GmbH, *STOE WinXPOW 210*, 2004, Darmstadt, Germany.
31 A. Boultif and D. Louër, *J. Appl. Crystallogr.*, 1991, **24**, 987–993.
32 W. I. F. David, K. Shankland, J. van de Streek, E. Pidcock, W. D. S. Motherwell and J. C. Cole, *J. Appl. Crystallogr.*, 2006, **39**, 910–915.
33 D. W. M. Hofmann, *Acta Crystallogr. B*, 2002, **58**, 489–493.
34 P. M. de Wolff, *J. Appl. Crystallogr.*, 1968, **1**, 108–113.
35 G. S. Smith and R. L. Snyder, *J. Appl. Crystallogr.*, 1979, **12**, 60–65.
36 M. D. Hanwell, D. E. Curtis, D. C. Lonie, T. Vandermeersch, E. Zurek and G. R. Hutchison, *J. Cheminformatics*, 2012, **4**, 17.

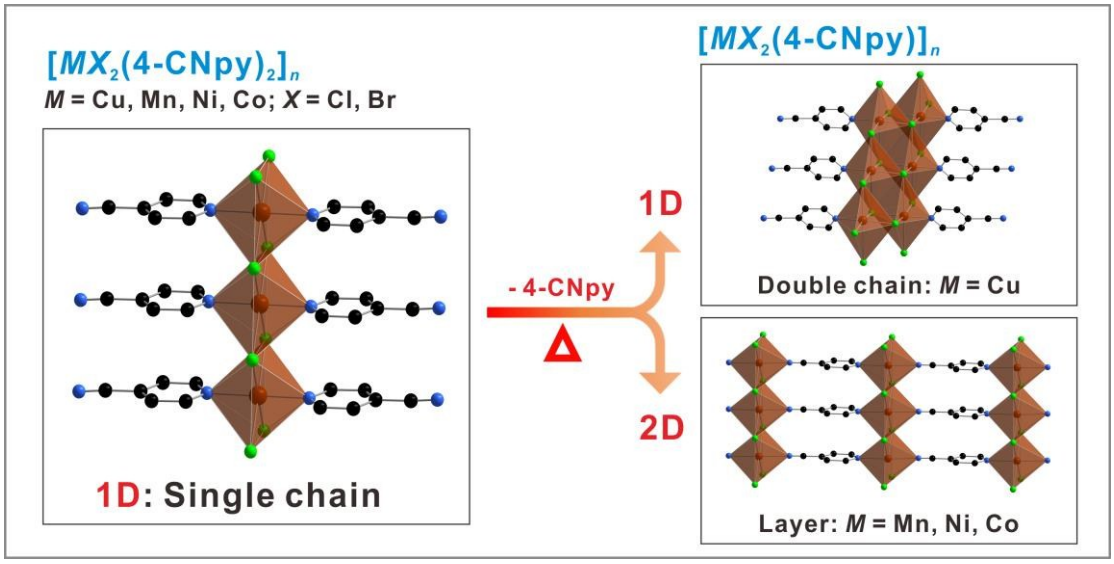

4-Cyanopyridine (4-CNpy) as monodentate ligand in single or double chains or as bidentate ligand in two-dimensional networks.